Long duration stabilization of porous silicon membranes in physiological media: Application for implantable reactors

Abdoullatif Baraket, Jean-Pierre Alcaraz, Chantal Gondran, Guillaume Costa, Guillaume Nonglaton, Frederic Gaillard, Philippe Cinquin, Marie-Line Cosnier, Donald Martin

HAL Id: hal-02370519

https://hal.science/hal-02370519

Submitted on 21 Jul 2022

Long Duration Stabilization of Porous Silicon Membranes in Physiological Media: Application for Implantable Reactors

Abdoullatif Baraket[1,†], Jean-Pierre Alcaraz[2, †], Chantal Gondran[3], Guillaume Costa[4], Guillaume Nonglaton[4], Frédéric Gaillard[4], Philippe Cinquin[2], Marie-Line Cosnier[4], Donald K Martin[2,*]

[1] ISA, Institut des Sciences Analytiques, Département LSA, 5, rue de la Doua, 69100 Villeurbanne, France.

[2] Université Grenoble Alpes / CNRS / TIMC-IMAG UMR 5525 (SyNaBi), Grenoble, France, Faculté de Médecine38706 La Tronche cedex - France.

[3] Univ. Grenoble Alpes, CNRS, DCM UMR 5250, F 38000, Grenoble, France

[4] CEA LETI Grenoble - DRT/DTBS, 17 avenue des martyrs, 38054 Grenoble cedex 9, France

* Corresponding Author: Prof D.K. Martin, don.martin@univ-grenoble-alpes.fr

† These authors (AB, J-PA) contributed equally to this work and are considered to be joint first-authors.

Abstract

The natural biodegradabilty of porous silicon (pSi) in physiological media limits its wider usage for implantable systems. We report the stabilization of porous silicon (pSi) membranes by chemical surface oxidation using RCA1 and RCA2 protocols, which was followed by a PEGylation process using a silane-PEG. These surface modifications stabilized the pSi to allow a long period of immersion in PBS, while leaving the pSi surface sufficiently hydrophilic for good filtration and diffusion of several biomolecules of different sizes without any blockage of the pSi structure. The pore sizes of the pSi membranes were between 5 and 20 nm, with the membrane thickness around 70 µm. The diffusion coefficient for fluorescein through the membrane was 2×10^{-10} cm^2 s^{-1}, and for glucose was 2.2×10^{-9} cm^2 s^{-1}. The pSi membrane maintained that level of glucose diffusion for one month of immersion in PBS. After 2 months immersion in PBS the pSi membrane continued to operate, but with a reduced glucose diffusion coefficient. The chemical stabilization of pSi membranes provided almost 1 week stable and functional biomolecule transport in blood plasma and opens the possibility for its short-term implantation as a diffusion membrane in biocompatible systems.

Keywords: porous silicon, surface modification, diffusion, stabilization

Glossary :

pSi: porous silicon; **APTES**: 3-aminopropyl-triethoxysilane; **PEG**: polyethylene glycol; **RCA1** and **RCA2**: Standard cleaning procedures 1 and 2 of silicon wafers from the "Radio Company of America"; **PBS**: phosphate buffer saline; **EIS**: electrochemical impedance spectroscopy; **GBFC**: glucose biofuel cell; **DRIE**: deep reactive ion etching; **FTIR** spectroscopy: Fourier Transform InfraRed Spectroscopy; **TCS**: 2-

[Methoxy(polyethyleneoxy)propyl]trichlorosilane; **CPE**: Constant Phase Element; **YFP**: Yellow Fluorescent Protein; **FITC**: fluorescein isothiocyanate; **SDS-PAGE**: Sodium Dodecyl Sulfate- PolyAcrylamide Gel Electrophoresis; **BSA**: bovine serum albumin; **DI** : Deionized water; **CAM**: Contact angle measurements; **SEM**: Scanning electron microscopy

Introduction

Porous silicon (pSi) is widely used in biomedical applications due its biocompatibility and many other attractive physical and chemical properties[1,2]. It is naturally biodegradable and it can be shaped into functionalized nanostructured materials to serve as drug nanocarriers, hence for biomedical applications it is used mainly for the development of biosensors[3] and drug delivery[4-6]. The surface of pSi degrades in physiological media due to factors such as pH, temperature, surface chemistry and porosity[7,8]. The freshly prepared pSi has an inherent hydride silicon structure (SiH_x, $x=1, 2 \text{ or } 3$), which is a very reactive chemical structure in physiological media[9]. The hydride silicon structure is transformed to orthosilicic acid ($Si(OH)_4$) in aqueous solutions in the physiological pH range. The kinetic parameters of degradation and resorption of pSi nanoparticles are the major key advantages for its use in systems for controled drug release.

Despite its usefulness in drug delivery due to its capability for controled degradation, the intrinsic properties of pSi of large hydraulic permeability and an efficient pore-size selectivity provide opportunities for exploring additional biomedical applications. Indeed, a pSi membrane would have major

advantages that include; *(i)* the high porosity that provides a large exchange surface, *(ii)* the size of the nanopores that allows for differentiate between small molecules and proteins, *(iii)* the possibility to modify the surface by doping or metal deposition to permit electrical conduction, and *(iv)* the capability for membrane stacking and packaging because the pSi membrane is integrally supported by non-porous silicon.

Nonetheless, the major hurdle for an implantable pSi membrane is to overcome its natural degradation in physiological solutions[10]. In these conditions the degradation of pSi usually results in a change of the membrane pore-size or a total blocking of those pores. The concomitant reduction in membrane thickness could offset such blocking of the pores, but such a degrading membrane would not provide a predictable diffusional flux. To overcome these problems several techniques to stabilize the pSi have been reported in the literature. These include molecular self assembly, chemical and plasma treatment, electroless deposition of metals or coating of biomaterials[11]. All of those surface modification methods have been developed by taking into account the pore sizes, the membrane thickness and the pore density. However, the most common techniques used to preserve the chemical structure of pSi are by oxidation or silanization. Thermal oxidation was reported as the better process to completely oxidize the pSi surface[12]. Salonen *et al*[13,14] have used isothermal microcalorimetry (IMC) to measure water adsorption/desorption at the surface of porous silicon for a humidity sensor application and have

reported IMC signals overtime which is interpreted as the stability of the surface. The diffusion across those membranes have not been tested.

Thermal oxidation requires an annealing of pSi at ~700°C under oxygen flow. At this temperature the pSi changes its structure and thereby the diffusional flux properties. It is possible to perform a back-bond oxidation at a lower temperature between 250°C and 450°C under flow of oxygen. Although the oxidation with this process generates hydroxyl groups on the pSi surface, the highly reactive hydride silicon groups on the pSi surface always remain[12]. Another soft technique to oxidize pSi using oxygen plasma has been reported by Jiang *et al*[15]. In their study, the authors have demonstrated that during the plasma process the oxygen ion concentration inside the membrane is proportional to the pore size and the pSi membrane thickness. For example, for narrow pores the oxygen ions cannot penetrate deeply into the membrane. Consequently, this technique can be only used for thin porous membranes. However, the fragile structure of pSi limits the optimum means of oxidation to be only that achieved by aqueous chemical treatments, since chemical aqueous solutions cross all the membrane and oxidize all pSi surfaces. Several liquid phase oxidations have been developed, including KOH, KNO_3, H_2O_2, H_2SO_4, and piranha solution (sulphuric acid + hydrogen peroxide)[16-19]. These oxidants transform the pSi surface into hydroxyl groups with a release of hydrogen.

In addition to oxidation, the pSi can also be silanized with different terminated silane groups for bio-functionalization or protection of its surface

for implantation. In this regards, Naveas et al[20] have reported an exhaustive study concerning the chemical stabilization of porous silicon using a silane-amine

3-aminopropyl-triethoxysilane known as APTES. In that study, the authors have made a comparison between an APTES-treated pSi that was previously oxidized by thermal and by chemical protocols. The amine terminated groups allow the grafting of several biomolecules on the pSi surface. Following the same principle Bragaru et al[21] have reported the APTES bio-functionalization of porous silicon using a combination of several oxidation protocols based on hydrogen peroxide. Although this silane reagent allows the possibility to graft a large range of biomolecules onto the pSi surface, it is not recommended for use in implantable devices due to the high nonspecific adsorption caused by amine groups of APTES with other biomolecules. For this reason a polyethylene glycol silane (silane-PEG)[22] was used as an alternative silane reagent for the passivation of implantable devices. PEG is known in the literature to minimise non-specific protein binding while leaving the surface hydrophilic. Several protocols have been developed for the PEGylation of pSi, including silylation and the functionalization of pSi with pegylated molecules. Baranowska et al[23] used silane-PEG-NHS to provide a homogeneous coating of biomolecules on the surface of pSi. This was made on pSi that was previously oxidized thermally by RCA1 and RCA2 protocols or by other oxidation processes[23-26]. In recent reports, the pSi surface has been modified by using PEG-silane on

slit-shaped pSi membranes and built an intravascular bioartificial pancreas device[27,28]. Langerhans islets were fed by blood flow from an arteriovenous bypass across the pSi membrane. The cells remained viable and active *in vitro* and *in vivo* under convective mass transport. The authors proved that the slit-shape structure of the pSi membrane was capable to maintain sufficient exchange of molecules with a 3-fold greater hydraulic permeability compared to existing polymer membranes. However, since those results were only reported for a short duration, the issue of degradability of the pSi membranes was not investigated and it remains an important issue to be resolved.

In the present research we investigate the means to stabilise pSi for its use in physological conditions, which in this study we mimicked using, initially, phosphate buffered saline (PBS) and then blood plasma. We stabilized the pSi from degradation while leaving the porous surface sufficiently hydrophilic to allow the circulation of buffers through the pSi membrane. Our protocols commenced with oxidation of the pSi membranes by piranha solution, sulfuric acid (H_2SO_4), hydrogen peroxide (H_2O_2), or RCA1+RCA2 protocols. Then, a silane monolayer with PEG-terminated groups has been optimized to cover the whole surface of pSi matrix, which will be in contact with the physiological medium. After each treatment the membranes were immersed in PBS solution to confirm that the treatment procedure did indeed stabilise the pSi. We confirmed that the pSi membranes were functional using diffusion experiments and 4-electrode electrochemical impedance spectroscopy (EIS), particularly

after incubating the silanized pSi membranes in blood plasma for long periods. The stabilization of pSi membranes in physiological media is very promising for packaging inside implantable devices. An example of potential usage of pSi that is stabilized against degradation is for the packaging of a glucose biofuel cell (GBFC)[29], as illustrated in figure 1. Our previous work indicates that the complete GBFC needs to be mechanically confined in a polymeric membrane to protect it from the body and to allow biofuel diffusion into the GBFC[29-31]. There are several challenges that need to be overcome for successful implantation of medical devices[32,33], but nonetheless the pSi membranes clearly provide good scope for additional smart packaging inside implantable devices that require diffusion of molecules.
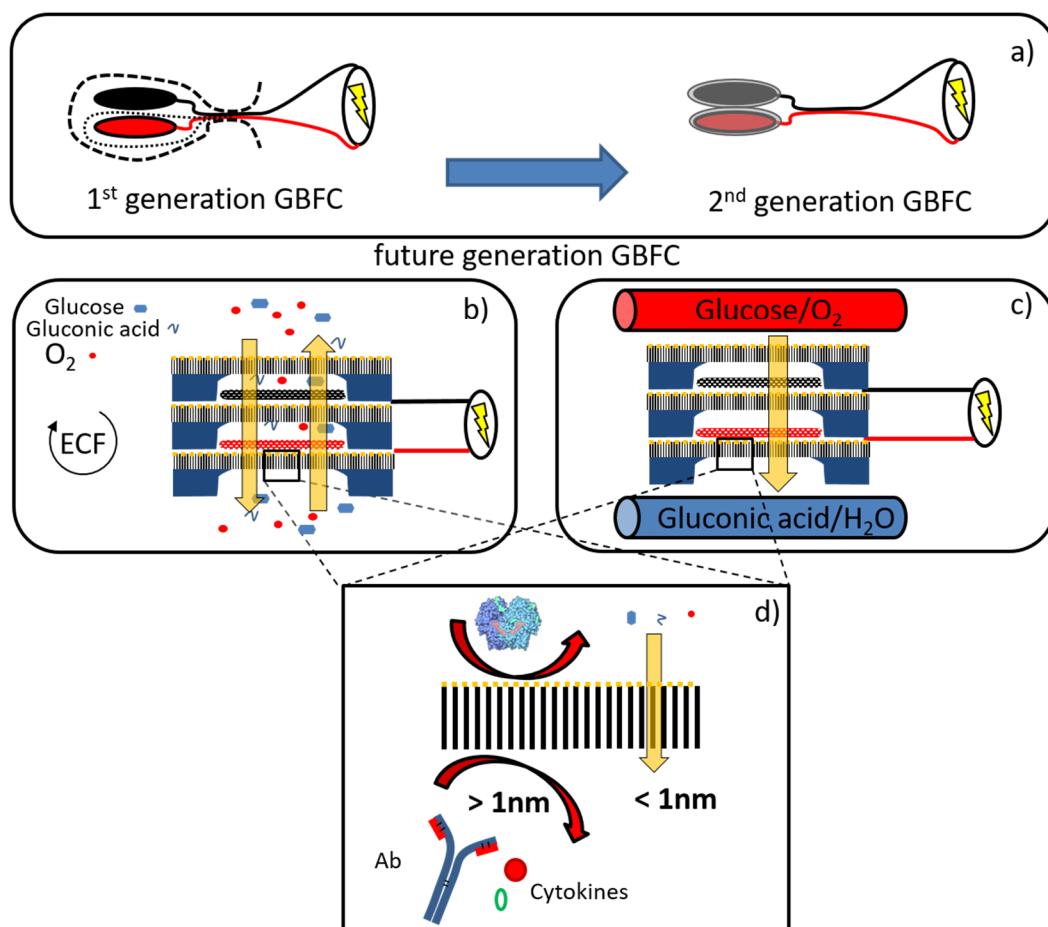
Figure 1: Schematic illustration of glucose Biofuel cell (GBFC) consists in 2 bioelectrodes, an anode (in black) and a cathode (in red) within which redox reactions occurs. The GBFC is powered by glucose oxidation at the anode and reduction of oxygen at the cathode. a) The *in vivo* proof of concept of the functioning was established by the use of a semi-permeable membrane in order to avoid enzymes and other associated small molecules to leak out. The 2nd generation uses a polymer coating onto the electrodes that limit the inflammatory response. b) and c) A future generation of GBFC with two conceptual illustrations of a nanoporous silicon membrane based implantable biofuel cell. The GBFC is packaged between 2 silicon chips within nanoporous membranes. b) The device can be implanted in the abdominal cavity where it is surrounded by extracellular fluid (ECF) as described in [30]. Substrates and products of the reaction freely diffuse across the membrane. The diffusion rate benefits from the movement of organs against each other in the abdominal cavity. Gold coated onto pSi (in yellow color) drives the collected current to the wires and optimize the current transfer from the enzymes. c) The device can be implanted in the arm of a patient as described in [27]. The ultrafiltrate flux of molecules is then generated across an arteriovenous graft and benefits from a natural pressure gradient between the two compartments. d) Zoom on nano pSi membrane: The nanoporosity is defined to allow small molecules and ions to pass through but avoid the access of antibodies and cytokines and prevents leakage of enzymes enclosed in the reservoir.

Results and discussion

Untreated nanoporous silicon membrane

Figure 2a shows the front-side and the back-side of an individual chip of 20mm x 20mm. The back-side of the membrane has a very hydrophobic character, indicated by the contact angle of ~130° (Figure 2b), due to the presence of hydrosilane bonds ($Si-H_x$, $_{x=1,2,3}$) on the porous surface. The droplet seems to be in the Wenzel state where the water impregnates the surface roughness. This chemical structure prevents the circulation of water through the membrane. In addition, the high roughness of the back-side of the membrane also contributes to the high hydrophobic character (Figure 2c). This rough structure was formed because of the deep reactive ion etching (DRIE) which is performed to open the membranes. Details of manufacturing

thenanoporous silicon membrane areprovided in the methods section and illustrated schemtically in Supplementary Figure S1.
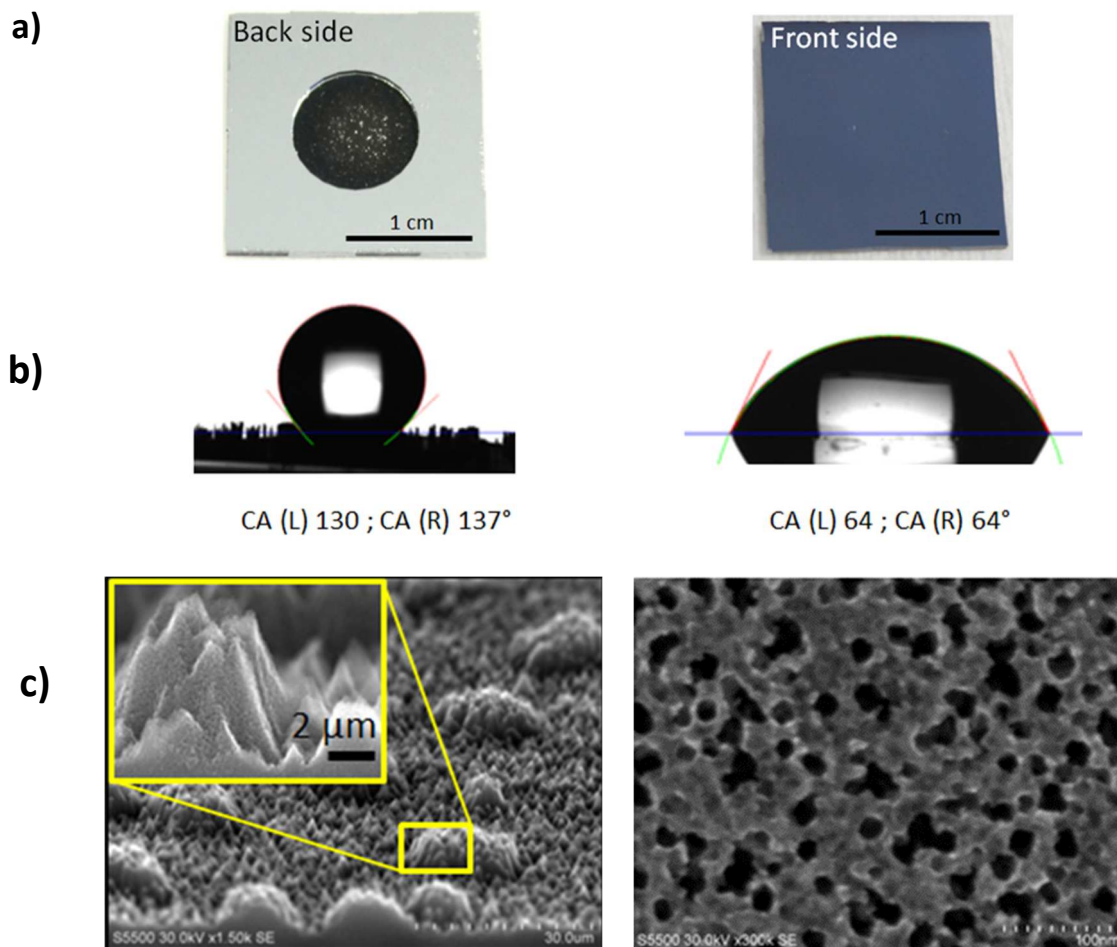

Figure 2: a) Different views of an individual pSi membrane back and front sides. b) Corresponding contact angles and profiles of the water droplet on the rough back-side of the membrane (left) and the smooth front-side of the membrane (right). c) SEM images of the back-side (left) showing the high roughness of the surface and the front side (right) of the membrane showing the surface of the pores.

The pSi can be pre-wet with ethanol in order to improve water circulation through the membrane[34]. In that regard Mery[35] has reported an exhaustive study of porous silicon wettability and surface energy using different ratios of ethanol/water mixtures. Although this technique has helped the circulation of water through the membrane it cannot be used for physiological medium due to the presence of ethanol, which can denature biomolecules present in

physiological media. Moreover, that process requires an inconvenient two-step procedure. More importantly, the freshly prepared pSi dissolves to orthosilicic acid in water or in physiological serum. The kinetics of pSi dissolution depends on the pore sizes as well as on the pH and the temperature of the medium[9] and thus prevents the use of this type of membrane as a diffusion barrier, even for short term use (order of minutes).

In the present work, we observed the dissolution of pSi in PBS (pH 7.4 at room temperature of 24°C) by formation of hydrogen bubbles on the surface of the porous membrane (Figure 3a) (see video in Supplementary Information). To overcome this problem of pSi dissolution, we tried four chemical protocols in order to protect the pSi surface. After each chemical treatment, the membranes were incubated in an aqueous PBS solution to ensure that there was no evolution of hydrogen bubbles (Figure 3b) and thus confirmed the the chemical stabilization of pSi.
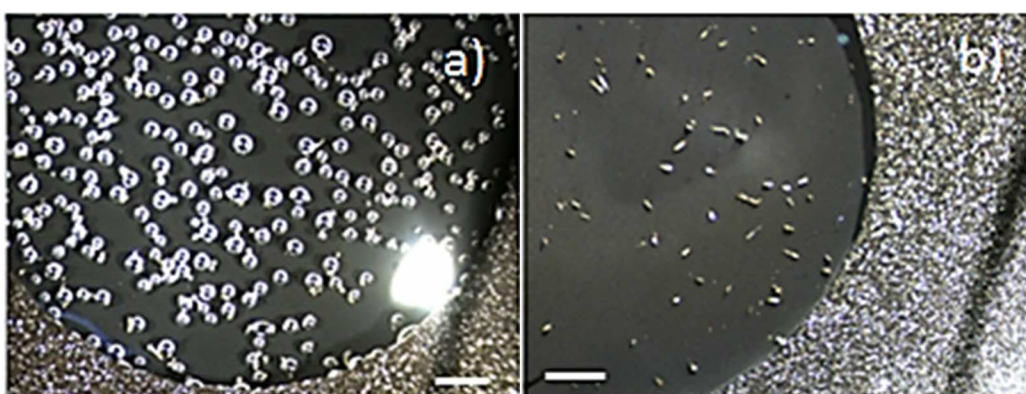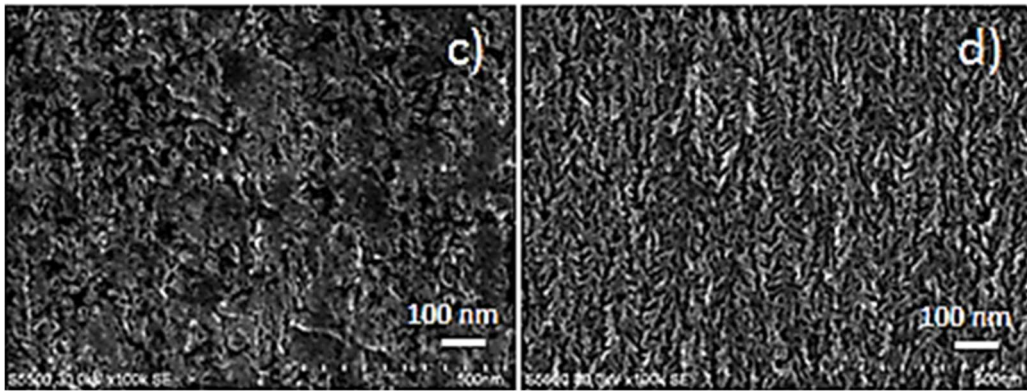
Figure 3: Upper panel: Macroscopic view of the rough surface of nanoporous membrane (Scale bar 1mm) a) hydrogen bubbles formation in presence of PBS onto an unstabilized pSi membrane. b) absence of hydrogen bubbles in presence of PBS for a stabilized pSi. Bottom panel: SEM cross sectional view of the membrane for (c) a totally collapsed structure of RCA oxidized porous silicon after three days in PBS, and (d) RCA oxidized and silanized with TCS at 1% after two months of its incubation in PBS.

Thermal stabilization treatment

Thermal stabilization has been tested for our pSi membranes. However, this process causes deformation and breaking of the membranes, due to the thin pSi membrane needed for optimal diffusion. Results are shown in the supplementary information (Figure S2-1).

Chemical stabilization

Several chemical protocols were used to stabilise the pSi membranes for use in physiological media. These chemical protocols were chosen in such a way that they did not change the geometry and the structure of silicon pores.

Piranha treatment

Although the piranha treatment gave good results in terms of surface oxidation and stabilization in PBS solution (absence of hydrogen bubbles), this protocol was not continued because it creates a marked deformation of the 70

12

µm membrane (Supplementary Figure S2-2). For example, in a diffusion application this may change the pSi structure, the pore size and thus the flux of biomolecules.

Sulfuric acid treatment

Treatment by sulfuric acid renders a hydrophilic behaviour of pSi. Gas bubbles continue to be visible even after many cycles of rinsing for long periods. Distinctive smell of hydrogen sulfur suggest hydrogen sulfide bubbles and sulfur contamination. In addition sulphuric acid is reputed in the literature to be very difficult to eliminate from supports after piranha treatment or directly after sulphuric acid treatment[36]. Moreover, this treatment changes significantly the density of the porous bulk (Supplementary Figure S2-3c and S2-3d), compared to the oxidation made by hydrogen peroxide, in which the porous structure remained open on all the membrane (Supplementary Figure S2-3a and S2-3b). Consequently, the oxidation with sulfuric acid was not continued.

Hydrogen peroxide treatment

In order to optimise the pSi oxidation with hydrogen peroxide, several combinations of parameters were made by changing the time of oxidation and H_2O_2 concentration. The oxidation time was varied from 1 to 30 hours, whilst the hydrogen peroxide was used at 35% or diluted in water (1:3). The treatment was followed by FTIR analysis of the pSi after different types of oxidation in

comparison with an unoxidized pSi membrane Figure S2-4a. The three peaks 2000, 2150 and 2200 cm^{-1} for only oxidized pSi, corresponds to the three forms of Si-H bonds which exist on the freshly prepared pSi. After 1hr of oxidation, these peaks decreased significantly and a large peak between 3000 and 3800 cm^{-1} appeared, which corresponds to OH bonds and highlights a significant oxidation of the pSi.

Nonetheless, this treatment by hydrogen peroxide for 1 hr was not sufficient to completely stabilise the pSi. This was confirmed by a weak formation of small hydrogen bubbles after 1hr of pSi immersion in PBS. Increasing the duration of oxidation increases the OH-peak and significantly decreases the Si-H peaks. The maximum oxidation state was achieved at 30hr of pSi oxidation at 30%. In these conditions, the oxidized pSi was sufficiently stabilized since no hydrogen bubbles were seen even after 4hr of pSi immersion in PBS. The oxidation with hydrogen peroxide has shown good preliminary results in terms of stability.

RCA1 and RCA2 treatment

To optimize the oxidation, RCA1 and RCA2 treatments were applied at different times with FTIR measurements performed after each RCA treatment to control the pSi oxidation. The Si-H peaks were greatly diminished after 5 min of RCA treatment. Significantly, after only 5 min of oxidation using RCA treatment similar results have been obtained when compared to those made by

30hr of oxidation using H_2O_2 (Supplementary Figure S2-4b). Normally, the RCA1 treatment was made at 65-80°C[37]. At this temperature with a concentrated ammonium hydroxide, the RCA1 contributes to the oxidation of pSi as well as to the dissolution of the formed silicon oxide. This was confirmed by an embrittlement of the porous membrane. In order to minimise this phenomenon the RCA1 step was made at room temperature followed by RCA2. In these conditions, no bubble formation was observed after three days on the porous silicon. Thus, RCA1 and 2 treatment were chosen for a deeper analysis.

Table 1 summarize the results obtained with all the oxidation protocols, including flux properties. Our qualitative observations on the membranes shows that thermally-treated or Piranha-treated membranes are strongly deformed and break easily. Sulfuric acid-treatment leads to sulfur contamination. The best results were obtained with H_2O_2 and RCA treatment. However, H_2O_2 was a long process so we have chosen to focus on RCA treatment.

Treatment	Presence of bubbles ?	Water pressure (mbar)	Flow (μL min^{-1})	General comments
Without treatment	Yes	100	-	No flow through
Thermally-treated	Yes	>50	-	Very fragile : Membrane break
H_2SO_4	Yes	100	0,33	Gas bubbles Porosity change
H_2O_2	No	100	0,49	Process of long duration
Piranha	No	100	0,35	Fragile : Deformed and broken membrane
RCA	No	100	0,54	Quick and robust

Table 1: Summary table showing the flux properties after the oxidation protocols used to stabilize the pSi membrane.

Silanization of membrane by 2-[Methoxy(polyethyleneoxy) propyl] trichlorosilane

Although that duration of stability is encouraging, for the aim to use pSi for implanted applications the pSi should be stable for a longer period in physiological media. To prolong the duration of stability, pSi membranes were silanized after their RCA oxidation. The silane-PEG 2-[Methoxy-(polyethyleneoxy)propyl]trichlorosilane (TCS) was used at 17 mM for one hour immediately after RCA oxidation as it was previously described. This treatment resulted in the preservation of the pSi surface structure for 1 month of incubation in PBS buffer (pH 7.4) supplemented with glucose (Figure 3d). This passivation of the pSi is very promising for implanted applications, such as for maintenance of the diffusion of biomolecules through the pSi membrane for a long period without any blocking of the membrane, or to act as a stable nanoporous support.

Characterization of the stabilized nanoporous silicon membrane

Ion permeability of the nanoporous silicon membrane

Ion permeability properties of the porous membrane were studied by electrochemical impedance spectroscopy with a 4-electrode configuration (Figure S3). Over time, the aging of an only-oxidized pSi membrane results in the decrease of permeability and an increase in the overall impedance. After two days, as seen in Figure 4c, there was a measurable diffusion which indicates that the oxidized-only

pSi membrane was still porous. Surprisingly, the diffusion decreased after storage in buffers. SEM images (Supplementary Figure S4-1) confirm that the pores became blocked after three days. Our explanation is that the structure is collapsing on itself before being dissolved. Indeed, SEM-EDX done after three days showed only oxygen and silicium peaks (see Supplementary Figure S4-2). The pSi degradation was also observed by a color change[38,39] (see Supplementary Figure S4-3). To demonstrate the beneficial effect of TCS treatment for the pSi membrane, the impedance responses were measured in PBS solutions over time for an only-RCA-oxidized membrane and a TCS-silanized membrane. Figure 4 shows these measurements and the line-of-best-fit for the equivalent circuit (inset panels in Figure 4).

Figure 4a shows the Nyquist plot of the impedance obtained on day-zero for an RCA-oxidized and a TCS-silanized membrane. For day-zero, the equivalent circuit consists of a parallel RC corresponding to the ion transfer resistance, $R_{interface}$, and the double layer capacity, $C_{interface}$, at the membrane/solution interface. A constant phase element (CPE) is used instead of capacitance to account for surface inhomogeneity of the interface between the solution and pSi membrane. The impedance of a CPE is given by $Z_{CPE} = Q^{-1}(j\omega)^{-\alpha}$ where Q is the amplitude of the CPE, ω is the angular frequency and α is the exponent which is a real number that varies between 0 and 1. When $\alpha = 1$ a purely capacitive behavior was observed (i.e. Q = C). The table presented in figure 3b shows values of $R_{interface}$, $C_{interface}$, the frequency at the top of the semicircle f and the parameter of surface homogeneity, α, obtained by the experimental data fitting. The resistances of the interfaces are of the same order of

magnitude even if the resistance of the interface with the TCS-silanized pSi membrane was slightly lower (62 ± 2 Ω for Ox pSi and 45 ± 2 Ω for TCS pSi). The slightly lower value after silanization, which reflects a better permeability of the membrane and suggests that the pores of the membrane are more hydrophilic after silanization. Although the double layer capacitances appear high in comparison to planar interfaces the porosity of the membrane most likely accounts for these apparently large capacitances.
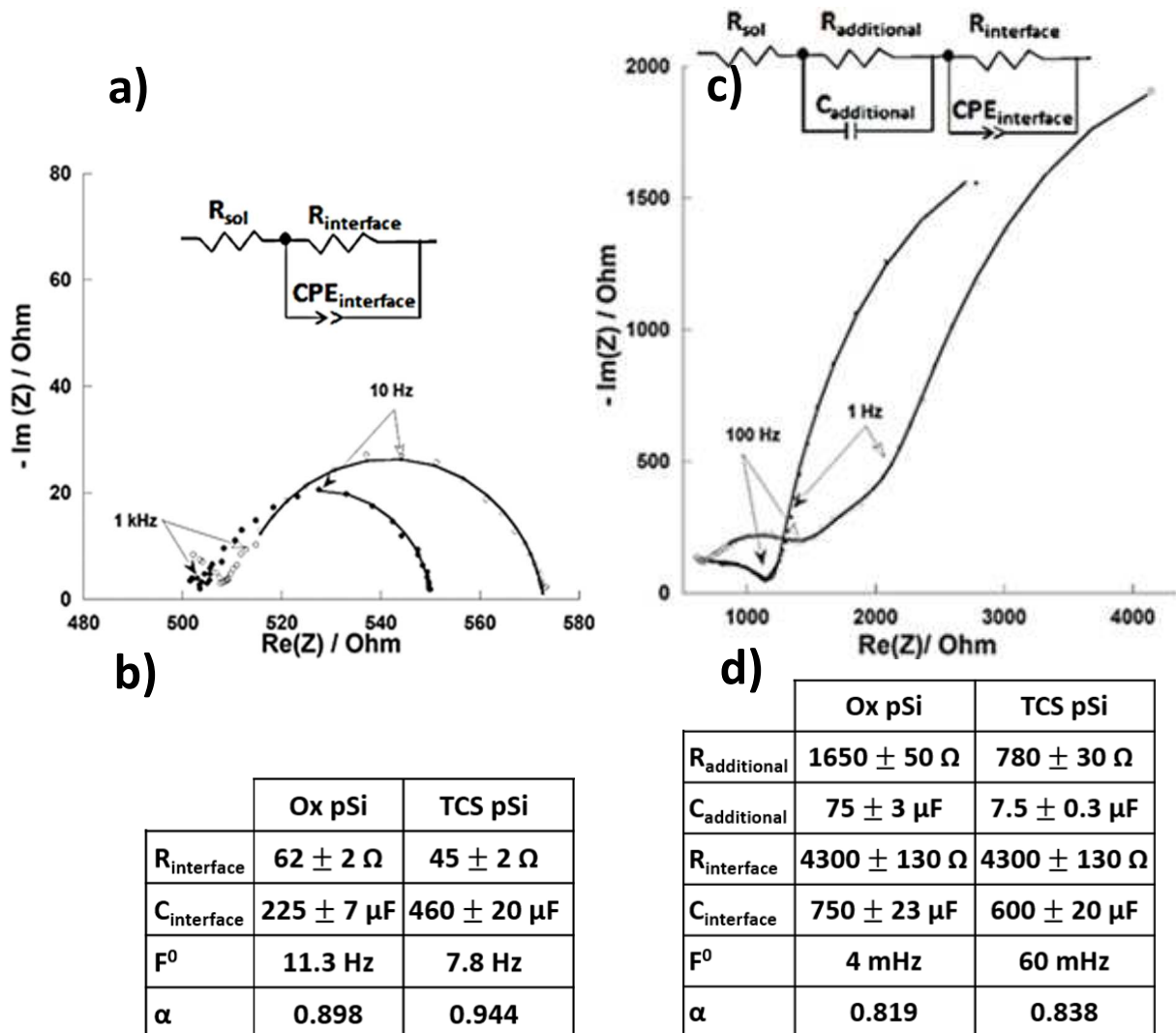

b)

	Ox pSi	TCS pSi
$R_{interface}$	62 ± 2 Ω	45 ± 2 Ω
$C_{interface}$	225 ± 7 μF	460 ± 20 μF
F^0	11.3 Hz	7.8 Hz
α	0.898	0.944

d)

	Ox pSi	TCS pSi
$R_{additional}$	1650 ± 50 Ω	780 ± 30 Ω
$C_{additional}$	75 ± 3 μF	7.5 ± 0.3 μF
$R_{interface}$	4300 ± 130 Ω	4300 ± 130 Ω
$C_{interface}$	750 ± 23 μF	600 ± 20 μF
F^0	4 mHz	60 mHz
α	0.819	0.838

Figure 4: a) Nyquist plot of RCA-oxidized (empty circles) and TCS-silanized membrane (filled circles) before PBS incubation. The fitted curves are showed with lines determined with the equivalent circuit in the box; b) corresponding electrical parameters before PBS incubation. c) Nyquist plot of RCA-oxidized (empty circles) and TCS-silanized membrane (filled circles) after PBS incubation: 2 days for the RCA-oxidized membrane and 30 days for the TCS- silanized membrane.

The fitted curves are showed with lines with the equivalent circuit in the box. d) corresponding electrical parameters after PBS incubation.

The presence of the TCS on the surface of RCA-oxidized membrane is confirmed by the increase in double layer capacity (225 ± 7 µF for Ox pSi and 460 ± 20 µF for TCS pSi). The parameter α is still high which confirms a high homogeneity of the interface between membrane and solution in the pores. Furthermore, the homogeneity of the interface has increased after silanization (0.898 for Ox pSi and 0.944 for TCS pSi). Figure 4c represents the Nyquist plots obtained for these membranes after 2 days of PBS incubation for the only-oxidized membrane and after 1 month of PBS incubation for the TCS-silanized pSi membrane. It can be seen that the overall impedance increases from about 500 to 2800 Ω after 1 month for a TCS-silanized pSi membrane while these changes are obtained after only 2 days (from 500 to 4000 Ω) without silanization treatment of the pSi membrane. The increase in impedance in both cases reflects a loss of permeability of the membrane over time, it being much faster without the silanization step. The equivalent circuit of the pSi membrane after the PBS immersion needed to be adjusted to account for the degradation of the pSi membrane. For example, after 1 month with a TCS-silanized pSi membrane (or 2 days with an RCA-oxidized membrane), the equivalent circuit required the inclusion of an additional parallel RC element to account for degradation of the membrane. The basis for this change in the equivalent circuit can be seen in Figure 4c, where a loop strongly decentered corresponding to this additional RC is seen, at high frequency, between the beginning of the impedance spectrum and the semicircle corresponding to the membrane/solution interface. Presumably a hydrated

silicon oxide layer partially covers the membrane/solution interface in the pores and poor ionic conduction of the hydrated silicon oxide layer brings up an additional loop on the Nyquist plot. The table presented in Figure 4d shows values of the equivalent circuit elements obtained by the experimental data fitting. For the additional parameters, which appeared during the degradation of the membrane over time, $R_{additional}$ is lower on the TCS-silanized pSi membrane (1650 ± 50 Ω for Ox pSi and 780 ± 30 Ω for TCS pSi). This suggests that the presence of TCS slowed the onset of the phenomenon associated with this resistance. $C_{additional}$ is lower on the TCS-silanized pSi membrane (75 ± 3 nF for Ox pSi and 7.5 ± 0.3 nF for TCS pSi). Here the unity of the additional capacitance is nanofaradic, which confirms the presence of an additional material which could be hydrated silicon oxide. In addition, the electrical and dielectric properties of the membrane solution interface (at low frequency on the Nyquist plot) have been heavily modified over time. $R_{interface}$ increases strongly for both membranes (69 times for Ox pSi and 95 times for TCS), which shows that the ion permeability of the porous membrane is diminished compared to day zero. The parameter α, is decreased (10 %) indicating a loss of homogeneity of the interface. The pores are not as much homogeneous. These results demonstrate that although the pores have been damaged over time by a hydrated silicon oxide layer the TCS-silanization treatment slows the development of this layer.

Pore size cut-off estimation using fluorescent probes

After the stabilization by RCA treatment and TCS silanization, the pSi membrane was tested for the filtration of different biomolecules with different sizes. In addition to pSi stabilization, these biological tests highlight the performance of these membranes in complex media without any blocking of pores by biomolecules or nonspecific bonding.

The theoretical volume of a globular protein can be calculated from the approximation published by Harpaz *et al*[40]:

$$\text{Vol. prot (Å}^3) = \text{molecular weight (g mol}^{-1}) \text{ x } 1.21$$

Assuming that the pores on one side are about 5 nm in diameter, it means that a globular protein with a molecular weight greater than 54,063 g mol^{-1} is unable to pass through the membrane.

Molecules	Weight g.mol^{-1}	Minimum sizes (nm)	Back side detection	Front side detection
Lipidot	>50 000	50	✓	✗
Yellow Fluorescent Protein (YFP)	27 000	2.4	✓	✗
Fluorescein isothiocyanate (FITC)	389.38	~1	✓	✓

Table 2: fluorescent biomolecules filtered by TCS-silanized pSi with their corresponding molecular weight and size (✓ visible, ✗ non detectable).

A first approximation of the pSi membrane cut-off was achieved by using 3 types of fluorescent molecules that were lipidots[41], purified Yellow Fluorescent Protein (YFP) and fluorescein isothiocyanate (FITC) (Table 2). The passage of the fluorescein FITC molecules through the pSi membrane was confirmed by a presence

of a high intensity of fluorescence on the front side of the membrane in contact with the transport buffer. The protocol used and the associated images are presented in Supplementary S5-1. Lipidot® nanoparticles of 50 nm diameter were unable to penetrate through the membrane and have been blocked at the back side of the membrane. This was confirmed by the absence of fluorescence in the buffer crossing the membrane. The same experiment was performed using a yellow fluorescent protein YFP, which has a cylindrical shape of 4.2 nm long x 2.4 nm diameter (Supplementary S5-2). This biomolecule was also filtered by the membrane since no fluorescence was observed on the front side into the eluted buffer. On the other hand, FITC was able to pass through the membrane. The smallest diameter of FITC is 0.943 nm (S5-2). We can conclude that the cut-off of those membranes is below 2.4nm, twice smaller than the observed pores by scanning electron microscopy, probably due to the quite complex geometry of the pores (Figure 2c and Figure 3d).

Protein bacterial lysate, which contains a large range of protein sizes, was used in the present study to test the filtering capabilities of the pSi membrane. After filtration or passive diffusion, the quantification of the proteins contained in the buffer was estimated on a SDS-PAGE. Despite the detection limit of the Coomassie blue (around 100 ng for 20-30 kDa proteins), no protein band can be seen after filtration or free diffusion and thus confirms the remarkable filtration capabilities of the pSi membrane (Supplementary Figure S5-3). However, the production of such membranes is quite complex with respect to existing filters based on disposable modified cellulose or polyesters used *in vitro*.

Diffusion of glucose and fluorescein in physiological media

Glucose and fluorescein were used to measure the passive diffusion properties of the pSi membranes, particularly whether the diffusion changes over time during long-term exposure to PBS or to blood plasma. The apparent permeability and diffusion coefficient of both glucose and fluorescein were calculated from the measurement of the flux of the probe used according to Fick's law of passive diffusion:

$$P = \frac{V_b}{AC_a} * (\frac{dC_b}{dt})$$

where (V_b) is the volume of the sampling chamber (B) (5 mL) (Supplementary Figure S6-1), (A) is the area of the membrane (0.785 cm²) exposed to buffer from both sides of the cell, (C_a) is the concentration (g /L^{-1}) of the probe in donor chamber (A), and $((dCb)/dt)$ is the slope of the plot $C_b=f(t)$. Figure S6-1 shows that glucose and fluorescein passively diffuse across the tested membranes. The diffusion coefficient (D) for the membranes was calculated from

$$D = Pl$$

where l is the thickness of the membrane (50 µm for cellulose acetate membrane and 70 µm for porous silicon membrane) and P is the permeability calculated from Fick's law.

During the 2 months of immersion in PBS there were 2 distinct periods of aging (Figure 5a and Supplementary S6-2). The measurements start after 15 days of

incubation in PBS. During the first month, from day 18 to day 33, the diffusion coefficient for TCS-silanized pSi was twofold greater than for cellulose acetate. The TCS-silanized pSi diffusion coefficients are 4.3×10^9 cm^2 s^{-1} for glucose (Figure 5a) and 2×10^{-10} cm^2 s^{-1} for fluorescein (Supplementary Figure S6-2). A summary of the results is presented in table 3.

		Glucose	Fluorescein
Molecular weight (g.mol^{-1})		180	332.3
Size (nm)		0.7 nm	~ 1 nm
Diffusion coefficient (cm^2 s^{-1})	Cellulose acetate (25 μm thick)	2.5×10^{-9}	1×10^{-10}
	TCS pSi (70 μm thick)	4.3×10^{-9}	2×10^{-10}

Table 3: Diffusion coefficients obtained after incubation 1 month in PBS or 1 week into blood plasma of TCS treated pSi membrane and 6-8 kDa cellulose acetate membrane.

Around 2 months, from day 55 to day 63, the diffusion decreases by a factor of 8 but the TCS-silanized pSi membrane remains porous with respect to glucose (Figure 5a) and fluorescein (Supplementary Figure S6-2). The diffusion coefficient drops to 15% of the initial value in both cases. For the cellulose acetate membrane, the diffusion coefficients for glucose and for fluorescein remained stable, albeit greater than for TCS-silanized pSi after 55 days.

We found a 1:20 ratio between glucose and fluorescein diffusion due to the structural difference in the probes used. The molecular weight of fluorescein is 2 fold greater than glucose, it is a negatively charged flat molecule, and the presence of aromatic rings makes it hydrophobic[42]. All these differences can explain that the diffusion of glucose is more than 20 fold greater than the diffusion of fluorescein.

The diffusion coefficient is in the same order as the 6-8 kDa cellulose acetate membrane that is well characterized as a dialysis membrane[43]. With the latter, a ratio of 1:25 is found between the 2 probes with glucose diffusion coefficient of 2.5 x 10^{-9} cm² s^{-1} for glucose and 1x 10^{-10} cm² s^{-1} for the fluorescein.

During this experiment, bovine serum albumin (BSA) was incubated in the donor chamber to evaluate the antifouling properties of the TCS-silanization. BSA is known in the literature for its character for easy adsorption onto several materials and subsequent difficulty in removal. However, the diffusion of either glucose or fluorescein through the TCS-silanized pSi membrane was not affected by the presence of BSA in the solutions. In comparison, diffusion of glucose and fluorescein through the only-RCA-oxidized pSi membrane was diminished in the presence of BSA in the solutions. For the only-RCA-oxidized pSi membrane we observed a white film on the surface, which indicated that fragments of BSA were adsorbed strongly onto the porous surface and thus blocked the membrane. (Supplementary Figure S6-1b). The chemical surface modification using TCS-silanization was sufficient to preserve the geometry of the porous silicon membrane and thus protect it from blocking by protein-containing buffers.

To extend these observations to other physiological media, the diffusion of glucose was tested after immersing RCA-oxidized and TCS-silanized pSi membranes in blood plasma (Figure 5b). Plasma is a more complex medium compared to PBS, with plasma containing 2 to 3 hundred types of proteins (60 to 80 g L^{-1}, approximately half being serum albumin), nutrients (glucose, lipids, and amino acids)

and metabolites (urea, bilirubin), and a great diversity of ions (mono and divalent) in a bicarbonate buffer. Even after storage in this complex blood plasma solution the TCS-silanized pSi membranes remained porous for more than 1 week when incubated in sheep plasma. As the degradation occurs faster in a complex medium like blood plasma than in phosphate buffer saline, it is very likely that proteins participate in or facilitate the clogging of the membrane.

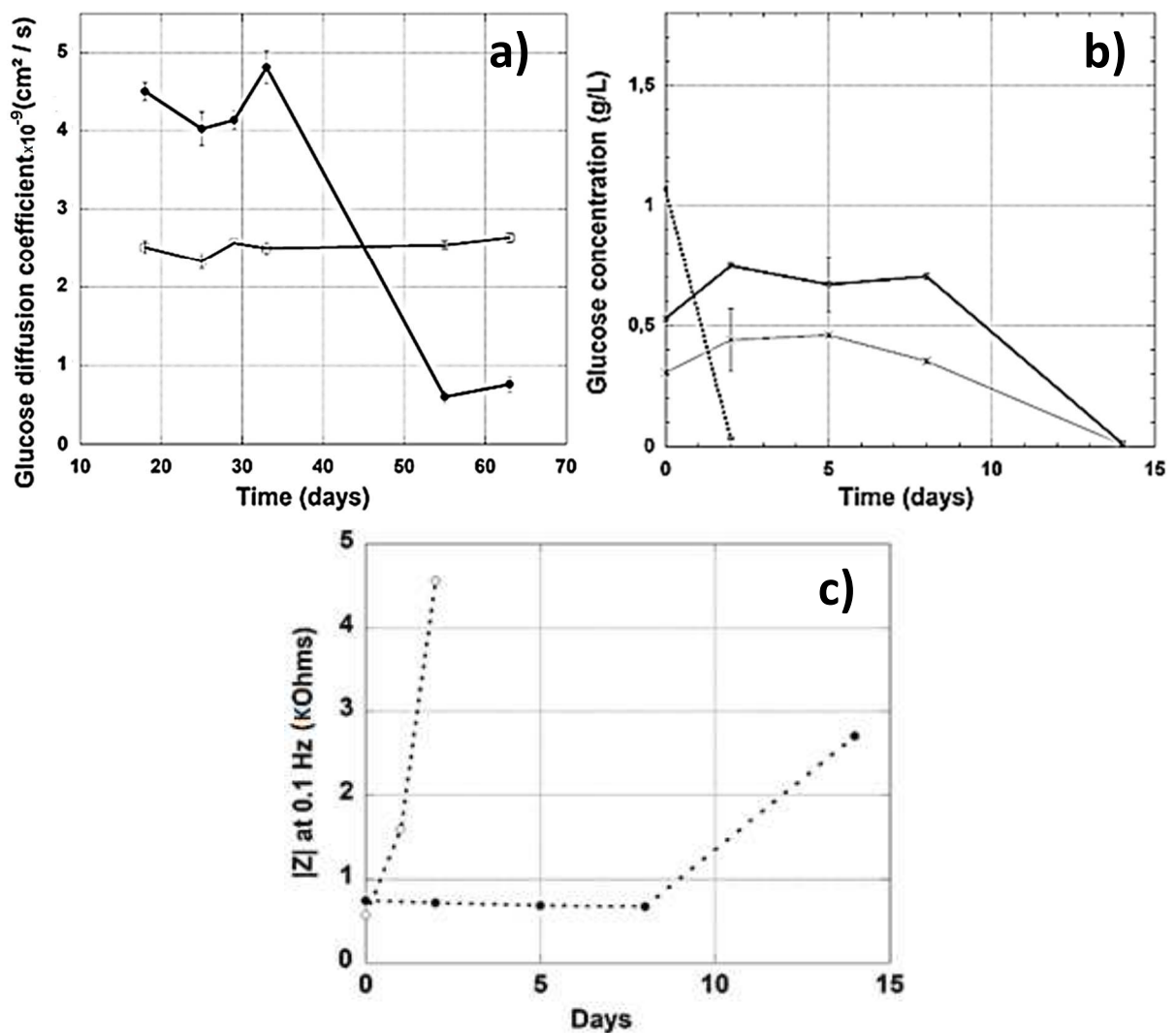This was not the case for the only RCA-oxidized pSi that became clogged after only two days.

Figure 5: Diffusion experiments during aging: a) Diffusion coefficients of glucose across 2 types of membrane and their stability during aging in PBS buffer. Filled circles refer to silanized nanoporous silicon membrane and empty circles refer to regenerated cellulose with 8kDa cut-off. Error bars correspond to 3 independent membranes. b) Representative membrane to show silanization

effect on glucose diffusion after plasma incubation from day 0 to day 14 with one oxidized membrane (dotted line) and 2 TCS silanized membrane (square and cross, solid line). The Y-axis shows the glucose concentration in the sampling chamber. c) Monitoring of the impedance at 0.1 Hz for a TCS silanized membrane (filled circles) versus oxidized membrane (empty circles) during plasma incubation.

These diffusion results confirm that the structure of the TCS-silanized membrane containing PEG affects the structure of the membrane, as we observed in the ionic permeability results using PEIS. Indeed, at day zero, half the amount of glucose is present in the sampling chamber of the two TCS-silanized membranes compared to the only-RCA-oxidized membrane (Figure 5b). This can be explained by the PEG-silane forming an additional layer that limits the diffusion of glucose and increases the binding of ions, consistent with our observation of the increased value of $C_{(interface)}$. Nonetheless, monitoring of the impedance showed that even after 2 weeks of incubation, the membrane is still porous towards ions (Figure 5c). Several impedance measurements were made between day zero and day 15. Figure 5c represents the low frequency impedance module (0.1 Hz) as a function of time for the TCS treated porous membrane and the only RCA oxidized porous membrane. The aging of the membrane is greatly slowed by the chemical surface modification of the pSi membrane using the TCS silane reagent. Although the total impedance has been multiplied by 4 in 15 days, the TCS silanized porous membrane retains good ion permeability.

Conclusions

Porous silicon nanoparticles are well adapted for drug delivery system because of their biocompatibility and biodegradability but it is quite challenging to stabilize a

porous silicon membrane for physiological use. To our knowledge, our work shows the first demonstration of the use of a nanoporous silicon membrane in a physiological environment for a long period of time by studying the aging of the membrane. We have made a quite complete characterization of this membrane using different physical and chemical techniques that include wettability, scanning electron microscopy, FTIR and EIS. We have also used diffusion experiments and electrochemical measurements in physiological media to test its permeability and its stability. By silanizing the membrane with a PEG-silane, we have obtained a good stabilization of the porous silicon membrane in physiological buffers for a long period of time. The pore sizes of these membranes were between 5 and 20 nm, with the membrane thickness around 70 µm. The diffusion coefficients through the membrane for fluorescein (2×10^{-10} cm^2 s^{-1}) or for glucose (4.3×10^{-9} cm^2 s^{-1}) remain stable for one month in PBS and 1 week in blood plasma. Moreover, unlike current membranes used for molecular diffusion in implantable devices, silicon simplifies the manufacturing process to easily create electrical connections. By comparison, cellulose acetate is very stable but induces inflammation (not biocompatible) and above all difficult to package. Similarly, a chitosan membrane does not induce inflammation (is biocompatible) but the electrical connections remain a difficulty. These issues are overcome by the use of nanoporous silicon membranes, which we have shown (see Supplementary Figure S7) can be metallized easily with conductive materials (e.g. gold). This opens the possibility for its short-term implantation as a biocompatible diffusion membrane. The nanoporous silicon membrane will also

be suitable for other application, in which packaging of silicon based devices requires a porous membrane to be included. Such devices could include, for example, gas sensors, filtration devices, or sensors that require specific filtration of molecules.

Methods

Reagents

Sulfuric acid 95%, hydrogen peroxide 35%, Hydrochloric acid (37%), ammonium hydroxide (30%), Fluorescein sodium salt, FITC Dextran, Bovine Serum Albumin (BSA), Glucose were purchased from Sigma-Aldrich. 2-[Methoxy(polyethyleneoxy) propyl]trichlorosilane (TCS) was purchased from ABCR, Germany. The glucose assay kit Glucose-GOD400 was purchased from Libios, France.

Preparation of porous silicon membranes

Porous silicon (pSi) material has been electrochemically generated in a hydrofluoric solution (HF) on a 200 mm diameter silicon substrate platform. A schematic of the process is displayed in supplementary (Figure S1). The 200 mm equipment is composed of cleaning and anodization chambers and it is fully automatic. Anodic dissolution of silicon was performed in a double tank cell where the front and back side of silicon wafer were immersed in the same electrolyte solution. This was made from a hydrofluoric acid/isopropanol mixture with 7 volumes of HF (50% weight) and 3 volumes of isopropanol. The porous silicon layer has been obtained on a <100>

boron-doped silicon substrate with a 10-20 mOhm Cm^{-1} resistivity. Anodization has been performed, at room temperature, in a galvanostatic mode with a current density equal to 17 mA cm^{-2}. A 100µm depth of pSi thickness has been achieved by adjusting the time process. In such conditions, a porosity gradient was observed throughout the depth profile and attributed to HF lowering concentration due to the low species replacement as process goes by. Afterward, DRIE process was performed from the back side of Si wafer through a photo-mask in order to open the porous silicon membrane. DRIE process was stopped once the pSi layer was achieved. The final thickness of porous membrane was ~ 70µm.

Chemical surface oxidation of pSi

<u>Sulfuric acid and Hydrogen peroxide</u>

Porous membranes were separately dipped in concentrated aqueous sulfuric acid (95%) and hydrogen peroxide (35% w/v in H_2O) at different times. A pre-wetting of porous surface membranes with ethanol was necessary to help sulfuric acid and hydrogen peroxide to cross the membranes. These were then rinsed three times with deionized (DI) water.

<u>Base Piranha</u>

The membrane were dipped in a mixture of hydrogen peroxide and sulfuric acid (3/4 : 1/4) for 1 hour. The same technique of pre-wetting with ethanol was used to help piranha solution cross the membrane. Afterward the membranes were rinsed three times with DI water

<u>RCA protocols</u>

In this step the membranes were dipped in the first aqueous solution called RCA1[34] made from a mixture of concentrated ammonium hydroxide (98%), hydrogen peroxide (35%) and water with a ratio of (1:1:5) at room temperature. These membranes were then rinsed 5 min in DI water for three times and dried with a smooth stream of compressed air in order to avoid breaking the membranes. Supplementary Figure S2-5 illustrates the RCA protocol. After RCA1 treatment, the membranes were dipped again in a second aqueous solution called RCA2 made from a mixture of hydrochloric acid (37%), hydrogen peroxide (35%) and water with a ratio of (1:1:5) at 65°C for 5 min. Finally, the membranes were rinsed in water for 5 minutes three times and dried with compressed air.

Silanization of pSi membranes

The oxidized porous membranes were immersed in a vessel purged with argon and filled with heptane solution containing 17 mM of 2-[methoxy(polyethyleneoxy)propyl]trichlorosilane (TCS). This static silanization was made at different times at room temperature. The membranes were then washed for 5 minutes in acetone, then in ethanol, and dried with a slight stream of nitrogen. Finally, the TCS treated membranes were left in an oven at 80°C during 30min in order to enhance TCS chemisorption onto the pSi surface.

Wettability

Contact angle measurements (CAM) were made to characterize untreated pSi and chemically treated pSi, using Kruss equipment (DSA100W, Germany). The contact angles were analyzed with deionized water and the measurements were repeated five times for each substrate.

Scanning electron microscopy (SEM)

Scanning electron microscope (SEM) characterization was made after each step in order to follow the evolution of the porous membrane. Membranes were cleaved and placed onto the holder of the SEM (5500a HITACHI).

Fourier-transformed infrared (FTIR) analysis

All spectra were measured with a Bruker IFS 55A FTIR spectrometer. The spectrometer employed a DTGS detector in transmission mode, sensitive to the infrared region from 4000 to 500 cm^{-1}. All spectra were recorded at a 4 cm^{-1} resolution and averaged using 32 scans. The spectrometer was monitored with a personal computer using OPUS software.

Four electrodes electrochemical impedance spectroscopy (EIS) analysis

The four-electrode impedance measurements were performed using the cell shown in supplementary (Figure S3) with a VSP300 Biologic potentiostat. The porous silicon membrane was clamped between two compartments with silicone flat gaskets. Each compartment was filled with 10-fold diluted PBS and contained a platinum electrode (current carrying electrode) and an Ag/AgCl electrode (reference

electrode). 51 measurements were conducted over a frequency region of 200KHz - 100mHz, with an applied voltage amplitude of 20mV peak to peak. The four-electrode technique is used to minimize the effects of electrode polarization on impedance measurements. Impedance plots were fitted to an equivalent electrical circuit using the ZView software (Scribner Associates, Inc).

Diffusion experiment procedure:

Fluorescence test

Optical fluorescence characterizations were performed using fluorescein (FITC) labelled biomolecules or recombinant Yellow Fluorescent Protein (YFP) to measure filtration through pSi membrane. 100µL of buffer containing FITC fluorescent biomolecules or 20 µl of 1.7µg µL^{-1} of YFP was dropped on the back side of the membrane and the optical observation was made from both the front and back sides (Supplementary Figure S5). The capillary force drives the liquid into the membrane. After 10 min the liquid can be seen on the other side. The fluorescence images were taken using a fluorescence microscope (Olympus Bx60 apparatus, equipped with 10×, 40× lenses and a monochrome camera USPT x10). Samples were observed by FITC fluorescence light which was excited with a 494(±25) nm band-pass filter and fluorescence from the sample was observed with a 518(±70) nm band-pass filter.

Dosage of biomolecules

The diffusion apparatus was a PermeGear Side-Bi-Side Cell (Supplementary Figure S6). It consists of two chambers, each of 5ml volume. The porous silicon

membrane was clamped between the chambers with two flat Teflon foam gaskets to avoid any leakage. The chamber (chamber B) was filled with only PBS.

Glucose and fluorescein diffusion analysis:

The kinetic diffusion was immediately started after filling the chamber (A) with 10 g L^{-1} glucose or 0.2 mg mL^{-1} fluorescein (FITC) in PBS solution. The temperature of the two chambers was controled by water jackets to be 25°C. The solutions in each chamber were well-mixed by stirring with magnetic fleas. Aliquots of 50 µL from the chamber (B) were then sampled at different times. Glucose concentration was obtained by using the glucose assay kit (LIBIOS). The absorbance and fluorescence were measured with a VICTOR spectrofluorometer microplate reader (Perkin Elmer). The same passive diffusion experiment was performed with dialysis 6-8 KDa cellulose acetate membrane as a reference for diffusion. For the experiment with sheep plasma the glucose concentration in the sheep plasma placed in chamber A was increased to 10 g L^{-1}, with chamber B containing PBS. Aliquots were sampled after 20 minutes of diffusion and glucose concentration in chamber (B) was obtained using the same glucose assay kit. The membranes were then incubated in sheep plasma supplemented with sodium azide (0.01%) to avoid any bacterial contamination during the 2 weeks of experiment.

Protein diffusion analysis:

A protein lysate from an *E.Coli* culture was prepared in distilled water by sonication and centrifugation at 15,000 rpm for 20 minutes. The protein concentration

was determined with the Thermo Scientific Pierce BCA Protein Assay Kit. Briefly, it combines the reduction of Cu^{2+} to Cu^{+} by proteins in an alkaline medium followed by the colorimetric detection of the cuprous cation chelated by bicinchoninic acid. A concentration of 1.5 g L^{-1} of total protein extract was used in the diffusion experiments. For the filtration experiment, a pressure of 0.1 bar was applied to the membrane. This value is compatible with an arteriovenous pressure differential[27]. A volume of 20 µL of protein lysate was extracted from the filtered buffer and analyzed on a 12 % SDS-PAGE colored with Coomassie brilliant blue and quantified by the BCA protein assay kit. For the passive diffusion experiment, in the PermeGear cell, a volume of 5 ml of PBS containing 5.5 g L^{-1} of lysate was added to chamber (A) against only 5 mL of PBS in chamber (B). After 40 min of passive diffusion, a sample of 300 µL of chamber B was precipitated with 80% acetone and 20 µl samples from both A and B chambers were put on a 15 % SDS PAGE colored with Coomassie brilliant blue and quantified by BCA protein assay kit.

YFP preparation:

The production of the recombinant yellow fluorescent protein (YFP) is described by Simkin *et al*.[44]. Briefly, the YFP was cloned in pQE plasmid, produced in *E.coli* M15, purified on Ni-NTA column and desalted on a PD10 column. The protein was stored at -80°C. The final concentration was 1.7 µg µL^{-1}.

References

[1] Z. Gaburro, N. Daldosso, L. Pavesi, in *Encyclopedia of Condensed Matter Physics*, Elsevier, Oxford, UK, 2005, pp. 391–401

[2] L. Canham, D. Malvern, *Properties of porous silicon INSPEC,* The Institution of Electrical Engineers, London, United Kingdom, **1997**

[3] S. Dhanekar, S. Jain, *Biosens. Bioelectr.* **2013**, *41*, 54

[4] N. Zilony, A. Tzur-Balter, E. Segal, O. Shefi, *Sci. Rep.* 2013, *vol*, 2499

[5] E.J. Anglin, L. Cheng, W.R. Freeman, M.J. Sailor, *Adv. Drug Del. Rev.* **2008**, *60*, 1266

[6] H.A. Santos, E. Mäkilä, A.J. Airaksinen, L.M. Bimbo, J. Hirvonen, *Nanomedicine*, **2014**, *9*, 535-554

[7] S.H.C. Anderson, H. Elliott, D.J. Wallis, L.T. Canham, J.J. Powell, *Physica Status Solidi (A)*, **2003**, *197*, 331

[8] X. Zhang, Y. Wang, Y. Zhao, L. Sun, *Mater. Sci. Eng. C*, **2017**, *77*, 19

[9] D. Xu, L. Sun, H. Li, L. Zhang, G. Guo, X. Zhao,L. Gui, *New J. Chem.*, **2003**, *27*, 300

[10] S. Moghaddam, E. Pengwang, Y.B. Jiang, A.R. Garcia, D.J. Burnett, C.J. Brinker, R.I. Masel, M.A. Shannon, *Nat. Nanotechnol.*, **2010**, *5*, 230

[11] P. Stroeve, N. Ileri, *Trends Biotechnol.*, **2011**, *6*, 259

[12] J. Riikonen, M. Salomäki, J. van Wonderen, M. Kemell, W. Xu, O. Korhonen, M. Ritala, F. MacMillan, J. Salonen, V.P. Lehto, *Langmuir*, **2012**, *28*, 10573

[13]   J. Salonen, V. Lehto, M. Björkqvist, E. Laine, L. Niinistö, *MRS Proc.*, **2000**, *638*, F14.19.1

[14]   J. Salonen, E. Mäkilä, *Adv. Mater.*, **2018**, *30*, e1703819

[15]   L. Jiang, S. Li, J. Wang, L. Yang, Q. Sun, Z. Li, *J. Nanomater.*, **2014**, *2014*, Article ID 526149, 6 pages

[16]   J.L. Cantin, M. Schoisswohl, A. Grosman, S. Lebib, C. Ortega, H.J. von Berdeleben, E. Vázsonhy, G. Jalsovszky, J. Erostyak, *Thin Solid Films*, **1996**, *276*, 76

[17]   F. Kozlowski, W. Wagenseil, P. Steiner, W. Lang, *MRS Proc.*, **1994**, *358*, 677

[18]   H.J. Fan, M.H. Kuok, S.C. Ng, H.S. Lim, N.N. Liu, R. Boukherroub, D. Lockwood, **2003**, *J. Appl. Phys.*, 94, 1243

[19]   I. Leontis, A. Othonos, A.G. Nassiopoulou, *Nanoscale Res. Lett.*, **2013**, *8*, 383

[20]   N. Naveas, V.T. Costa, D. Gallach, J. Hernandez-Montelongo, R.J.M. Palma, J.P. Garcia-Ruiz, M. Manso-Silván, *Sci. Technol. Adv. Mater.*, **2012**, *13*, 045009

[21 A. Bragaru, M. Simion, M. Miu, T. Ignat, I. Kleps, V. Schiopu, A. Avram, F. Craciunoiu, *IEEE Proc. Int. Semicond. Conf (CAS)*, **2007**, 1, 147

[22]   A. Papra, N. Gadegaard, N.B. Larsen, *Langmuir*, **2001**, *17*, 1457

[23]   M. Baranowska, A.J. Slota, P.J. Eravuchira, M. Alba, P. Formentin, J. Pallarès, J. Ferré-Borrull, L.F. Marsal, *J. Colloid Interface Sci.*, **2015**, *452*, 180

[24] L. Britcher, T.J. Barnes, H.J. Griesser, C.A. Prestidge, *Langmuir*, **2008**, *24*, 7625

[25] N.H. Voelcker, Y.L. Khung, S.J. McInnes, M.A. Cole, *Proc. SPIE BioMEMS Nanotechnol.*, **2007**, *6799*, 679909

[26] S.P. Low, K.A. Williams, L.T. Canham, N.H. Voelcker, *Biomaterials*, **2006**, *27*, 4538

[27] S. Song, G. Faleo, R. Yeung, R. Kant, A.M. Posselt, T.A. Desai, Q. Tang, S. Roy, *Sci. Rep.*, **2016**, *6*, 23679

[28] B.J. Feinberg, J.C. Hsiao, J. Park, A.L. Zydney, W.H. Fissell, S. Roy, S, *J. Membr. Sci.*, **2017**, *536*, 44

[29] A. Zebda, S. Cosnier, J.P. Alcaraz, M. Holzinger, A. Le Goff, C. Gondran, F. Boucher, F. Giroud, K. Gorgy, H. Lamraoui, P. Cinquin, *Sci.Rep.*, **2013**, *3*, 1516

[30] P. Cinquin, C. Gondran, F. Giroud, S. Mazabrard, A. Pellissier, F. Boucher, J.P. Alcaraz, K. Gorgy, F. Lenouvel, S. Mathé, P. Porcu, S. Cosnier, *PloS One*, **2010**, *5*, e10476

[31] S. El Ichi, A. Zebda, J.P. Alcaraz, A. Laaroussi, F. Boucher, J. Boutonnat, J., N. Reverdy-Bruas, M.N. Belgacem, P. Cinquin, D.K. Martin,. *Energy Environ. Sci.*, **2015**, *8*, 1017

[32] A. Zebda, J.P. Alcaraz, P. Vadgama, S. Shleev, S.D. Minteer, F. Boucher, P. Cinquin, D.K. Martin, *Bioelectrochemistry*, **2018**, *124*, 57

[33] J.P. Alcaraz, P. Cinquin, D.K. Martin, *Biotechnol. J.*, **2018**, 1800102

[34] A.G. Pel'menshchikov, G. Morosi, A. Gamba, *J. Phys. Chem.*, **1992**, *96*, 7422

[35] E. Mery, *Ph.D Thesis*, L'Institut National des Sciences Appliquées de Lyon, **2006**

[36] P. Resnick, C. Adkins, D. Kittelson, T. Kuehn, R. Gouk, Y. Wu, P. Clews, C. Matlock, Mechanistic studies of SC-1 particle removal and post piranha rinsing, *UCPSS, International Symposium on Ultra Clean Processing of Silicon Surfaces*, **1996**, *3*, 195

[37] W. Kern,D.A. Puotinen, *RCA Rev.*, **1970**, *31*, 187

[38] M.J. Sailor, J.R. Link, *Chem. Commun.*, **2005**, *21*, 1375

[39] E.C. Wu, J.H. Park, J. Park, E. Segal, F. Cunin, M.J. Sailor, *ACS Nano*, **2008**, *2*, 2401

[40] Y. Harpaz, M. Gerstein, C. Chothia, *Structure*, **1994**, *2*, 641

[41] J. Gravier, F.P. Navarro, T. Delmas, F. Mittler, A.C. Couffin, I. Texier, *J. Biomed. Optics*, **2011**, *16*, 096013

[42] H.G. Burghoff, K.L. Lee, W. Pusch, *J. Appl. Polym. Sci.*, **1980**, *25*, 323

[43] S. Sato, S.W. Kim, *Intern. J. Pharmaceut.*, **1984**, *22*, 229

[44] A.J. Simkin, J. Gaffé, J.P. Alcaraz, J.P. Carde, P.M. Bramley, P.D. Fraser, M. Kuntz, *Phytochemistry*, **2007**, *68*, 1545

Acknowledgements

Author contributions statement

AB and MLC conceived and conducted the pSi modifications and the filtration experiments.

FG conceived and manufactured the pSi.

GN and GC conceived and conducted the pSi surface modifications.

JPA, CG and DKM conceived, conducted and analyzed the ion permeability experiments.

JPA, DKM, PC conceived, conduct and analyzed the diffusion experiments.

AB and JPA wrote and all authors reviewed the manuscript.

AB and JPA contributed equally to the work.

Conflict of Interest

No author has any competing financial nor non-financial interest in this work.